The mass and size of Herbig disks as seen by ALMA (Corrigendum)

Stapper, L.M.; Hogerheijde, M.R.; Dishoeck, E.F. van; Mentel, R.

The mass and size of Herbig disks as seen by ALMA
(Corrigendum)

L. M. Stapper[1] , M. R. Hogerheijde[1,2], E. F. van Dishoeck[1,3], and R. Mentel[1,4]

[1] Leiden Observatory, Leiden University, PO Box 9513, 2300 RA Leiden, The Netherlands
 e-mail: `stapper@strw.leidenuniv.nl`
[2] Anton Pannekoek Institute for Astronomy, University of Amsterdam, PO Box 94249, 1090 GE Amsterdam, The Netherlands
[3] Max-Planck-Institut für Extraterrestrische Physik, Giessenbachstrasse 1, 85748 Garching, Germany
[4] School of Physics, University College Dublin, Belfield, Dublin 4, Ireland

In Stapper et al. (2022), which presents Atacama Large Millimeter/submillimeter Array (ALMA) archival continuum images of a sample of Herbig Ae/Be stars, an incorrect data file was accidentally used for one target, R CrA. As a result, a detection was erroneously reported for this source. Using the correct image results in a non-detection of millimeter flux for R CrA and an associated upper limit on the mass. This results in only minor changes in many of the values reported in Stapper et al. (2022), and none of the conclusions from Stapper et al. (2022) are affected.

R CrA has been removed from Fig. 2, see Fig. 1, and the entry of R CrA in Table 1 in Stapper et al. (2022) changes in Table 1. Figure 3 changes only marginally, see Fig. 2, the low-mass end of the distribution goes down slightly further. This changes the log-normal fitting results from a mean of 1.34 to 1.32 and a standard deviation of 0.53 to 0.57, both given in $\log_{10}(M/M_\oplus)$. The confidence intervals do not change. The mean dust mass for the Herbigs mentioned in Sect. 4.2 changes from 39 ± 6 $M_\oplus$ into 38 ± 5 $M_\oplus$. The percentage of disks with masses above 10 $M_\odot$ should be 63% instead of 67%.

Due to the non-detection, the radius is not known and the cumulative distributions of the dust radii presented in Fig. 6 change, see Fig. 3. The first of the p-values mentioned in the last paragraph of Sect. 4.3 changes from 1.8×10^{-4} into 9.5×10^{-5}, the second value reported does not change.

The mean dust mass of the unresolved disks mentioned in Sect. 5.1 changes from 25 ± 5 $M_\oplus$ into 19 ± 3 $M_\oplus$. Because no radius is known, R CrA is removed from Fig. 7, see Fig. 4. The modified dust mass distribution of the group I and group II Herbig disks is shown in Fig. 5, only the distribution of the group II disks changes slightly. Table 4 should have a mean of 0.61 instead of 0.63 and a standard deviation of 0.68 instead of 0.67; the confidence intervals do not change. Lastly, the corrected values of the frequency, beam size, and root-mean-square noise (RMS) of the observation in Table C.1 can be found in Table 2.

References

Ansdell, M., Williams, J. P., van der Marel, N., et al. 2016, ApJ, 828, 46
Ansdell, M., Williams, J. P., Trapman, L., et al. 2018, ApJ, 859, 21
Barenfeld, S. A., Carpenter, J. M., Ricci, L., & Isella, A. 2016, ApJ, 827, 142
Cleeves, L. I., Öberg, K. I., Wilner, D. J., et al. 2016, ApJ, 832, 110
Meeus, G., Waters, L. B. F. M., Bouwman, J., et al. 2001, A&A, 365, 476
Stapper, L. M., Hogerheijde, M. R., van Dishoeck, E. F., & Mentel, R. 2022, A&A, 658, A112
van der Marel, N., & Mulders, G. D. 2021, AJ, 162, 28
van Terwisga, S. E., van Dishoeck, E. F., Ansdell, M., et al. 2018, A&A, 616, A88

Table 1. Coordinates and spectral types of the Herbig stars used in this work and the calculated Band 6 and 7 flux densities and dust masses of each Herbig disk.

Name	RA$_{J2000}$ (h:m:s)	Dec$_{J2000}$ (deg:m:s)	Sp.Tp.	Group	$F_{cont.}$ (mJy)	M_{dust} ($M_\oplus$)	$R_{dust, 68\%}$ (au)	$R_{dust, 90\%}$ (au)	inc (°)	PA (°)	Ref.
R CrA$^\alpha$	19:01:53.7	−36:57:09	B5	II	<65.8	<13.2	–	–	–	–	18, ϵ

Table 2. Project IDs of the data used in this work with the corresponding observation frequency of the continuum data.

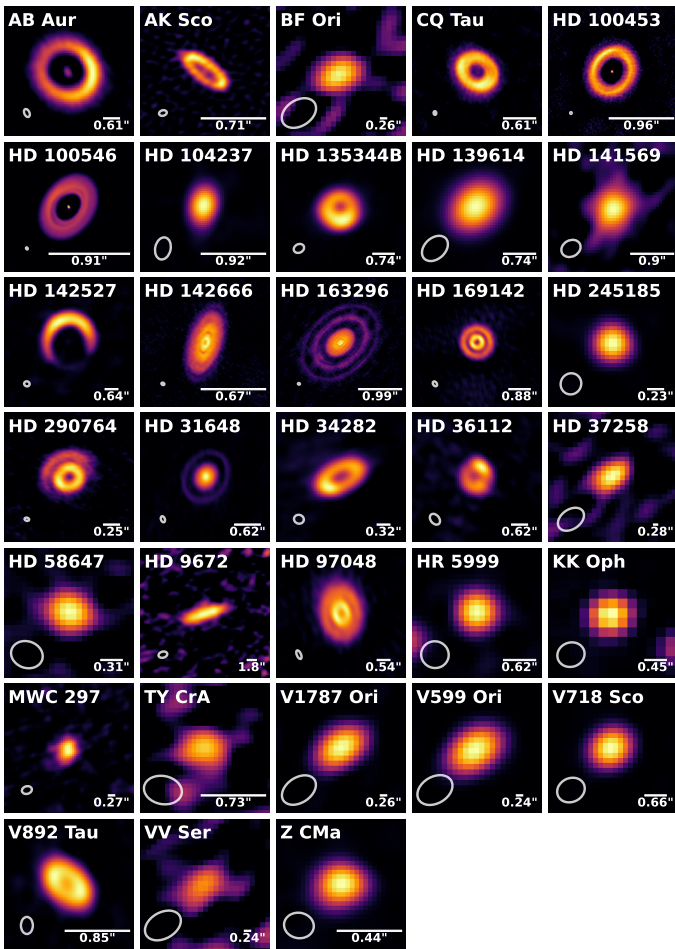| Name	ν (GHz)	Beam ('')	RMS (mJy beam^{-1})	Project ID
R CrA	231.32	7.48 × 4.68	11.3	2018.A.00056.S

Fig. 1. ALMA Band 6 and 7 continuum images of all objects. The size of the beam is shown in the *bottom left* of each plot and a scale bar of 100 au in size together with the angular scale in arcseconds is shown in the *bottom right*. Each image is normalized with an asinh stretch to make the fainter details of the disk more visible. HD 53367, HD 176386, and R CrA, which are not detected, are not shown.
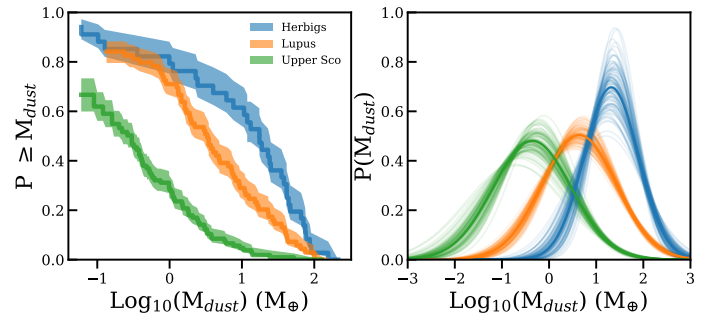

Fig. 2. *Left*: cumulative distribution functions of the dust masses contained inside the disks of our Herbig sample, Upper Sco (Barenfeld et al. 2016) and Lupus (Ansdell et al. 2016). *Right*: log-normal fit through the cumulative distributions. The solid line represents the best-fit distribution, while the light lines show a sub-sample of distributions from a bootstrapping method, showing the spread in possible fits.
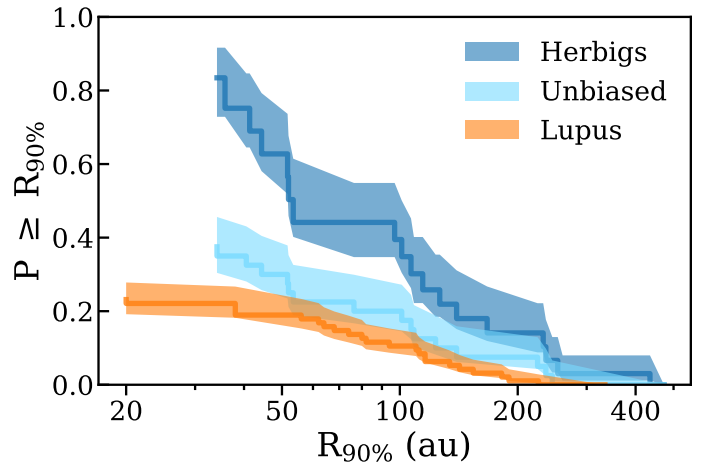

Fig. 3. Cumulative distribution functions of the 90% dust radii of the Herbig and Lupus samples (Ansdell et al. 2018). The unbiased distribution is made by assuming that all unresolved and unobserved disks are smaller than or equal in size to the smallest disk present in the sample.
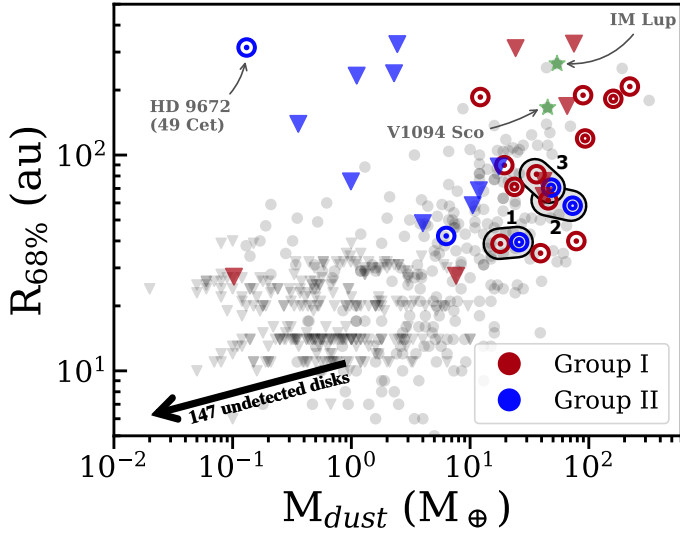
Fig. 4. $R_{68\%}$ radius plotted against the dust mass for the full sample in this work. Unlike Fig. 3, we use $R_{68\%}$ values here for consistency with the work of van der Marel & Mulders (2021). The Herbig disks are divided into the Meeus et al. (2001) group I and II disks. Disks with one (⊙) and two or more (◎) (visible) rings are indicated as well. The upper limits on the radius are plotted as triangles. The grey scatter points and radius upper limits are the T Tauri disks of van der Marel & Mulders (2021). The large arrow shows the range of upper limits on the undetected disks. Three pairs of Herbig group I and II disks are circled and numbered 1–3; these are further discussed in Sect. 5.4 and Fig. 10 in Stapper et al. (2022). For extra context, the positions of the large T Tauri disks IM Lup and V1094 Sco are shown as green stars (Ansdell et al. 2016, 2018; van Terwisga et al. 2018; Cleeves et al. 2016).
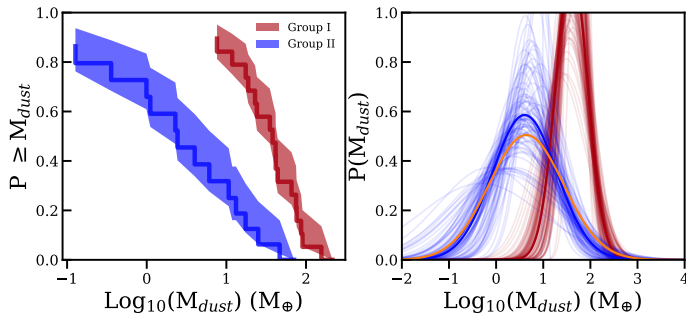

Fig. 5. *Left*: cumulative distributions of the dust masses of the group I and group II sources. *Right*: log-normal fit through the cumulative distributions. The solid line represents the best-fit distribution, while the light lines show a sub-sample of distributions from a bootstrapping method, showing the spread in possible fits. The orange log-normal distribution shows the best-fit distribution of Lupus shown in Fig. 2.